Planar AFM macro-probes to study the biomechanical properties of large cells and 3D cell spheroids

Laura Andolfi [a,*], Silvio L.M. Greco [a], Domenico Tierno [a,b], Roberto Chignola [c], Monica Martinelli [d], Elena Giolo [d], Stefania Luppi [d], Ines Delfino [e], Michele Zanetti [a,b], Alice Battistella [a,b], Giovanna Baldini [f], Giuseppe Ricci [d,f,*], Marco Lazzarino [a]

[a] Istituto Officina dei Materiali IOM-CNR, Basovizza, 34149 Trieste, Italy
[b] University of Trieste, 34100 Trieste, Italy
[c] Department of Biotechnology, University of Verona, Verona, Italy
[d] Institute for Maternal and Child Health, IRCCS Burlo Garofolo, Trieste, Italy
[e] Department of Ecological and Biological Sciences, Tuscia University, Viterbo, Italy
[f] Department of Medical, Surgical and Health Sciences, University of Trieste, Italy

ARTICLE INFO

Accepted 28 May 2019

Keywords:
Atomic force microscopy
Biomechanics
AFM-probes
Oocyte
Tumor spheroid
In vitro-fertilization

ABSTRACT

The ability to measure mechanical response of cells under applied load is essential for developing more accurate models of cell mechanics and mechanotransduction. Living cells have been mechanically investigated by several approaches. Among them, atomic force microscopy (AFM) is widely used thanks to its high versatility and sensitivity. In the case of large cells or 3D multicellular aggregates, standard AFM probes may not be appropriate to investigate the mechanical properties of the whole biological system. Owing to their size, standard AFM probes can compress only a single somatic cell or part of it. To fill this gap, we have designed and fabricated planar AFM macro-probes compatible with commercial AFM instruments. The probes are constituted of a large flat compression plate, connected to the chip by two flexible arms, whose mechanical characteristics are tuned for specific biological applications. As proof of concept, we have used the macro-probes to measure the viscoelasticity of large spherical biological systems, which have a diameter above 100 μm: human oocytes and 3D cell spheroids. Compression experiments are combined with visual inspection, using a side-view configuration imaging, which allows us to monitor the sample morphology during the compression and to correlate it with the viscoelastic parameters. Our measurements provide a quantitative estimate of the relaxation times of such biological systems, which are discussed in relation to data present in literature. The broad applicability of the AFM macro-probes can be relevant to study the biomechanical features in any biological process involving large soft materials.

Statement of Significance

The understanding of the role of physical factors in defining cell and tissue functions requires to develop new methods or improve the existing ones to accurately measure the biomechanical properties. AFM is a sensitive and versatile tool to measure the mechanical features from single proteins to single cells. When cells or cell aggregates exceed few tens of microns, AFM suffers from limitations. On these biological systems the control of the contact area and the application of a precise uniform compression becomes crucial. A modification of the standard cantilevers fabrication allowed us obtaining AFM macro-probes, having large planar contact area and spring constant suitable for biological investigations. They were demonstrated valuable to characterize the mechanical properties of large hierarchical biological systems.

* Corresponding authors at: Institute for Maternal and Child Health, IRCCS Burlo Garofolo, Trieste, Italy (G. Ricci).
E-mail address: andolfi@iom.cnr.it (L. Andolfi).

1. Introduction

Cell mechanics has been demonstrated to be relevant in a number of biological processes such as disease and inflammation [1,2], mechanosensation [3–5] and embryo development [6]. The mechanical characterization of a single cell is highly demanded for the evaluation of cell physical state regarding cancer detection and cell therapy [7,8], cancer cell aggressiveness [9,10], and quality of the gametes [11,12]. Nowadays, many techniques exist to measure the mechanics of individual cells. The most common ones are: micropipette aspiration [13], optical tweezers [14,15], atomic force microscopy (AFM) [16], parallel-plate rheometry [17] and microfluidic methods useful to provide high throughput measurements [18]. These techniques need to be coupled to adequate models to describe the cell mechanical properties. Common simple models describe cells as linear and uniform viscoelastic solids or shell–liquid core (or liquid drop) bodies: in the former case elastic and viscous properties belong indistinctly to the whole structure, in the latter one a pure tensile membrane encloses a pure viscous Newtonian fluid [19].

As long as relatively small individual cells are concerned, AFM offers an unrivaled versatility and sensitivity, and for these reasons it is widely used for the determination of the cell mechanical properties. Standard or modified (bead or wedged) AFM probes were used to indent, confine and compress a single cell, to investigate the mechanical characteristics of the cell [20,21] and of its intracytoplasmic structures [22]. The mechanical properties of individual somatic cells in isolation are mainly determined by the biophysical properties of the cytoskeleton and of the cell membrane.

Some biological systems have a scale larger than a single somatic cell. In the case of mammalian oocytes (diameter about 100 μm) additional structures contribute to their mechanical properties such as the zona pellucida (ZP), an extracellular membrane that surrounds the ooplasm. In general biological systems, are characterized by mechanical properties that depend also on the interactions between the nearby cells and with the extracellular matrix, as in multicellular aggregates (having a size above 100 μm diameter), which are relevant to investigate physiological and pathological processes. Unfortunately, the AFM investigation of these larger biological systems is limited by the size of standard AFM probes. Although the tip size of AFM probes can be increased, by gluing large beads up to 50 μm in diameter to the cantilever, this is still not ideal to obtain a large uniform and stable contact area to homogeneously and reproducibly compress a large biological system (above 100 μm). By using the beads, the compression measurements on such kind of samples would be locally dominated by the shape of the indenter, which could not be appropriate to detect the mechanical characteristics of the whole large biological system and of all the structures which it includes.

So far, the mechanical properties of these biological systems have been typically investigated by micropipette aspiration [23,24] or microplate rheology [25,26]. In micropipette aspiration technique, a suction pressure is generated in the pipette, as result a side of the cell is deformed by a series of steps of increasing pressure. The cell deformation into the pipette is measured using video microscopy. In the microplate rheology technique, the uniaxial displacement of the rigid microplate in the z-axis allows uniform deformation of the cell, which is optically monitored by a camera. These systems, although have provided insights into the mechanical characteristics of such biological systems, have several limitations. For instance, in the aspiration pipette approach both the inner diameter and focusing error of the micropipette need optical correction, similarly the micropipette taper needs measuring and compensating [27], while the microplate rheology, which can probe the whole cell mechanical response, does not have the force sensitivity required to carefully describe the biomechanical phenomena [28]. Instead the AFM can be used to directly measure or apply forces, from piconewton to micronewton range, on spatially defined areas with a fine control in z positioning, from the subnanometre to several tens of micrometres.

An ideal tool for the investigation of the mechanical properties of large biological systems should combine the sensitivity of AFM with the planar geometry providing for a large contact area and the extension depth of microplate compressor, which enables the application of uniform stress over a large vertical extension. Here in order to combine all these characteristics in a single approach, we design and fabricate dedicated AFM macro-probes compatible with commercial AFM apparatus. The probe consists of a large rigid squared plate connected to the bulk support with two thin flexible arms, which behave like an ideal spring and can be used to apply/measure the compression forces, as standard AFM cantilevers. We demonstrate the use of the AFM macro-probes for stress relaxation measurements of 3D tumor spheroids and human oocytes, correlated with microscopic visualization. These two biological systems, although physiologically very different, share some fundamental features: large size as compared to somatic cells, spherical shape and a complex ultrastructural organization. Our findings demonstrate that these AFM macro-probes are well suited to characterize the mechanical features of large biological systems, thus providing the possibility to improve the knowledge about the role of mechanics in fundamental biological processes such as meiosis, cell aggregation, tissue development in the early stage of tumor progression.

2. Macro AFM-probes design and fabrication

The structure of the AFM macro-probes was designed to match the geometrical constraints imposed by biological samples. To get uniform contact with a spherical object having a diameter $\geq$100 μm, a square area with side length of 300 μm was chosen. The mechanical parameters of the macro-probe were optimized through an analysis with finite element modeling (COMSOL Multiphysics). We designed a 3D model of the chip, including the base, using legs of the macro-probe having different lengths (100–400 μm) and widths (20–100 μm), which provide different mechanical characteristics (i.e. spring constant and stiffness). The base of the rectangular legs is the position where the stresses, caused by the compression of the spherical objects, occur. To estimate the stiffness of the whole system parametric simulations with varying loads (10–1000 nN) on a circular area in the center of the square plate were performed (Fig. 1A). The mechanical simulations allowed establishing the geometrical features that provided an effective spring constant of ~7 N/m, which enable to compress easily a large heterogeneous biological sample. As result, the selected geometry of the AFM macro-probe appears to be a square area of 300 × 300 μm in size connected to the solid chip with two cantilever arms 100 μm long and 100 μm wide (Fig. 1B).

The main fabrication steps are shown in Fig. 2A. On a silicon wafer (thickness 500 μm), covered by a layer of silicon nitride with a thickness of 2 μm on both sides, a thin layer of chromium (100 nm) was deposited by sputtering on both sides. One side of the wafer was spun coated with a photoresist (SPR 220 1.2) sensitive to UV radiation. Afterwards, a glass mask with the bottom side of the macro cantilevers was positioned on top of the photoresist, which was exposed to UV radiation to impress the pattern (exposure), and then immersed in the appropriate solvent to develop the resist (developing). After removing the resist, the chromium was patterned using the appropriate etching solution (Cr wet etching). As a result, the chromium was patterned with the designed shape and parts of the silicon nitride were left unprotected. An

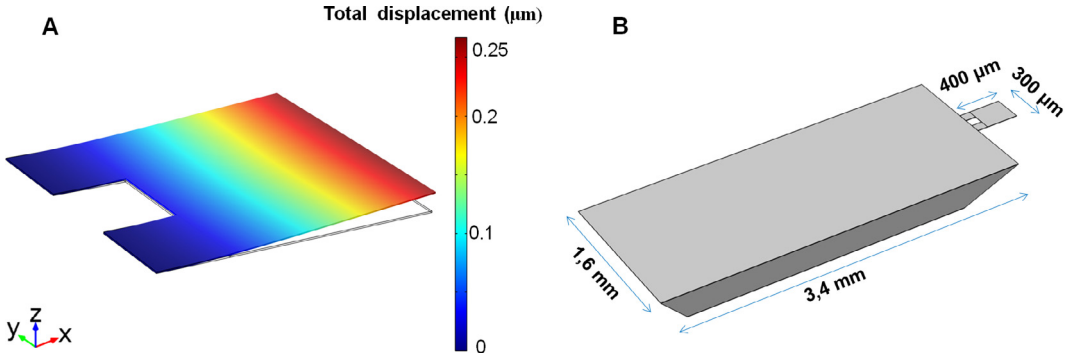

Fig. 1. Finite element simulation of the macro-probe deflection (A); the 3D representation of total displacement is scaled by a factor 200 to better visualize the probe deformation, while the colour bar indicates the real displacement values. Illustration of the 3D model of the chip exposing the AFM macro-probe (B). (For interpretation of the references to colour in this figure legend, the reader is referred to the web version of this article.)

etching step by reactive ion etching (RIE) with CF4/O2 plasma (dry etching) allowed eliminating the exposed nitrate with the resulting exposure of the silicon underneath, which was then etched by immersing the wafer in a heated 30% KOH solution until reaching a depth of 450 μm (Si wet etching). The pattern impressed on the silicon nitride included alignment holes which were punched after the silicon etching; these holes allowed the correct positioning of the top side mask (Back Side). The previously described process was repeated on the other side of the wafer (Front Side). The etching of the residual silicon layer was the final step to obtain the chips with the suspended silicon nitride macro-probe.

In order to correct the cantilever mounting tilt, common to every AFM set-up and provide a parallel and uniform compressing surface a polymeric wedge was added to the probe following the protocols described by Stewart and co-workers [29]. The wedge was fabricated using an UV-curable optically transparent glue: NOA 73 (Norland Optical Adhesive). A tiny drop of NOA73 (approximately less than 2.5 μl) was placed on a hydrophobic support (PTFE) that allowed to keep the drop confined. Then the probe, mounted on the AFM glass cube, was slowly brought into contact with the drop and illuminated with UV laser light (λ = 375 nm) for 1 min (see movie S1). The resulting macro-probe with the wedge is shown in Fig. 2B and C. Since the Young modulus of NOA 73, once cured, is 11 MPa, a factor thousand less than silicon but a factor thousand stiffer than cells, we assumed it infinitely rigid with a negligible effect on the evaluation of cellular mechanical properties. Finally, the macro-AFM probes were coated with poly-L-Lysine (500 μg/ml incubation for 2 h at room temperature) (Sigma-Aldrich) to facilitate biological samples adhesion.

2.1. Macro AFM probes calibration

The spring constant was calibrated by the spring on spring method [30]. In this procedure a cantilever with known spring constant was used as reference. The spring constant of the macro-AFM probe (*Kc*) was calculated according to the equation:

$$Kc = Kr\left(\frac{Sr}{S} - 1\right)$$

where *Kr* is the elastic constant of the reference cantilever, *Sr* is the sensitivity (nm/V) of the combination of macro-probe and reference cantilever, and *S* is the sensitivity of the macro-probe. As reference it is possible to use any commercial AFM cantilever; in our experiments we used PPP-FM cantilevers from Nanosensors with a nominal spring constant 0.5–9.5 N/m. Its spring constant was previously evaluated by the thermal noise procedure. The AFM macro-probe was mounted on the AFM-glass cube and the laser was aligned on its centre. The macro-probe was first pressed against the reference cantilever to obtain *Sr,* with the reference cantilever tip positioned in the centre of the macro-probe and then against the edge of the reference chip to obtain *S*. The AFM macro-probes (n = 10), used in this article had a spring constant average value of (1.7 ± 0.4)N/m (mean ± sem). However, the specific k value of each macro-probe was separately evaluated before every experiment with the biological sample.

3. Experimental application and data analysis

3.1. Stress-relaxation measurements and side-view imaging by AFM set-up

Stress-relaxation measurements were performed by using a NanoWizard II Atomic Force Microscope (JPK Instruments, Berlin, Germany) mounted on top of an Axiovert 200 inverted microscope (Carl Zeiss, Jena, Germany). To visualize the biological systems during measurements a side-view cantilever holder was used (JPK Instruments, Berlin, Germany). The holder bears a mirror positioned in front of the cantilever with an angle of 45°. By moving the mirror on top of the optical axis of the optical microscope lens, a reflected side-view image of the cantilever and the probed object can be recorded. In these measurements the cell to be measured was placed on the edge of a glass step to avoid crashing the side-view mirror on the sample support during cantilever approach. To this purpose, a stepped coverslip was fabricated by gluing a microscope glass slide (1 mm thick) into a plastic cap of a petri-dish (35 mm diameter) using NOA 73 optical adhesive (Norland Products). A coverslip 0.17 mm thick, previously coated with polydimethylsiloxane (PDMS) to create a hydrophobic surface, was then glued on top of the first overhanging by half of its size. Finally each support was rinsed in milli Q water, then with pure ethanol, and subsequently dried with a nitrogen flux.

A drop of medium (about 20 μl) containing a single oocyte or a single tumor spheroid was positioned close to the edge of the step. Thanks to the coverslip hydrophobicity the drop does not spread on the surface thus facilitating a rapid optical localization of the sample.

By using the optical transmission mode microscope integrated with the AFM microscope (top-view), the AFM macro-probe was positioned on the top of the oocyte/spheroid to allow for an accurate sample positioning. Afterward the AFM macro-probe was brought into contact with the oocyte/spheroid for less than 1 min to allow its binding at the probe centre lower side. At this stage the petri-dish was filled with medium using a syringe. Then the oocyte/spheroid was lifted from the surface and allowed establishing a stable adhesion to the probe for less than 5 min. This procedure allowed catching a single oocyte/spheroid, which could be then

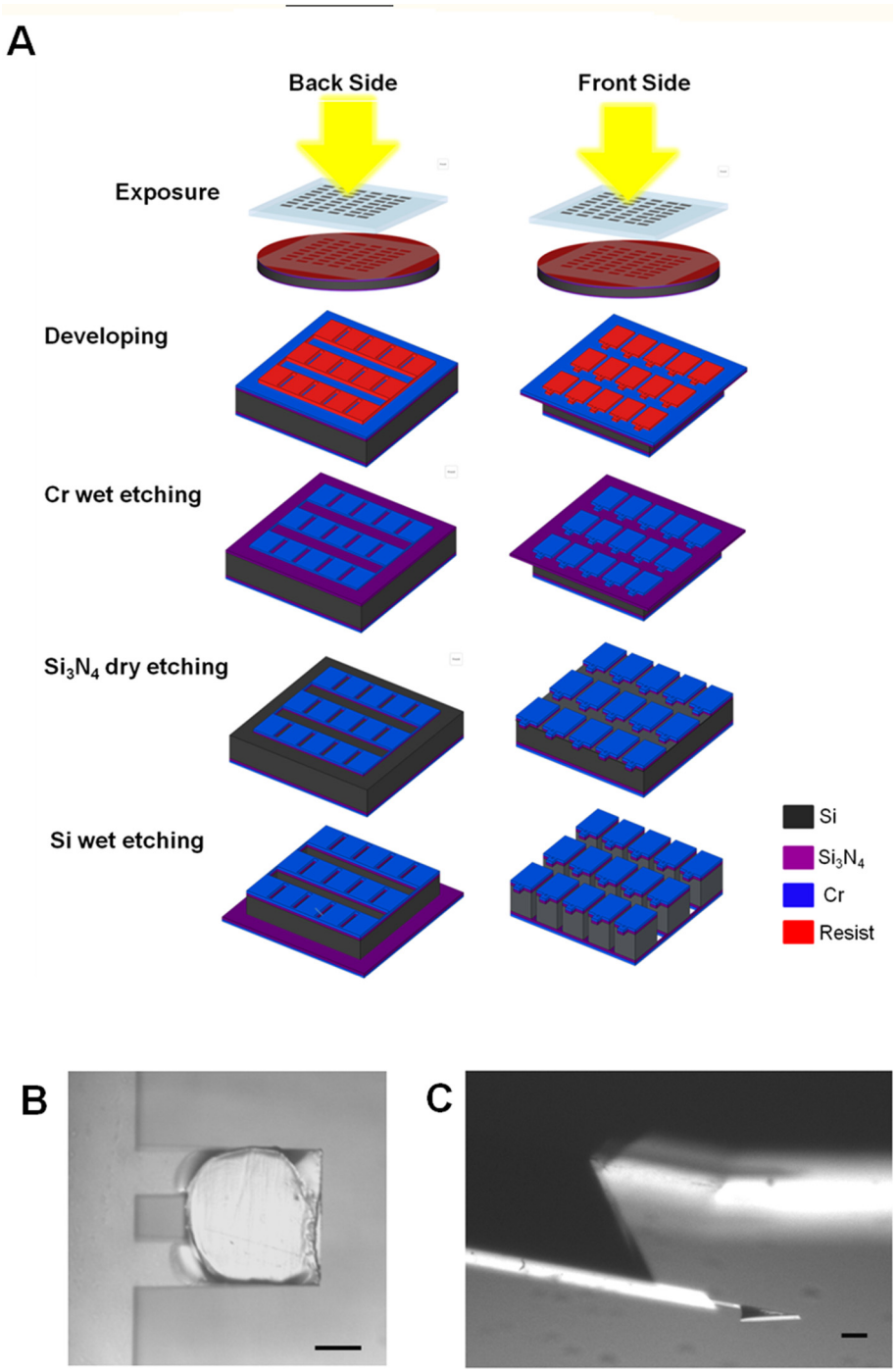

Fig. 2. Sketch illustrating all the steps of the fabrication procedure of the AFM macro-probes (A); visualization of the resulting macro-probe after the wedge formation: optical microscopy images top view (B) and side-view (C). Bar 100 μm (B); Bar 200 μm (C).

moved easily on the edge of the glass coverslip for measurements. At this stage the imaging was switched to a side-view imaging modality by illuminating the sample laterally as shown in Fig. 3A.

A CellHesion module (JPK Instruments, Berlin, Germany), which extends the vertical range of the AFM from 15 μm up to 100 μm, was used to compress the large biological objects. Stress-relaxation curves were collected by lowering the sample immobilized on the probe beyond the contact position. In the case of oocyte, the z piezo was lowered of 20 μm beyond the contact point with 2 μm/s speed. A closed-loop piezoelectric control was used to keep the z positioning constant for 30 s or 60 s. Afterward the probe was retracted to the initial position. On each oocyte between 3 and 5 curves were acquired. For spheroids the measurements were performed similarly. In this case the z piezo was lowered of 25 μm beyond the contact point and held constant for 120 s. On each spheroid between 5 and 10 curves were acquired. For side-view imaging, a 10X objective (Zeiss) was used. Side illumination was provided by an optical fiber lamp (X-Cite series 120). During measurements, images were recorded every second, with 100 ms integration time, by a DVC camera.

All the details about the cell line used for 3D tumor spheroids generation and their culture and human oocytes retrieval and their

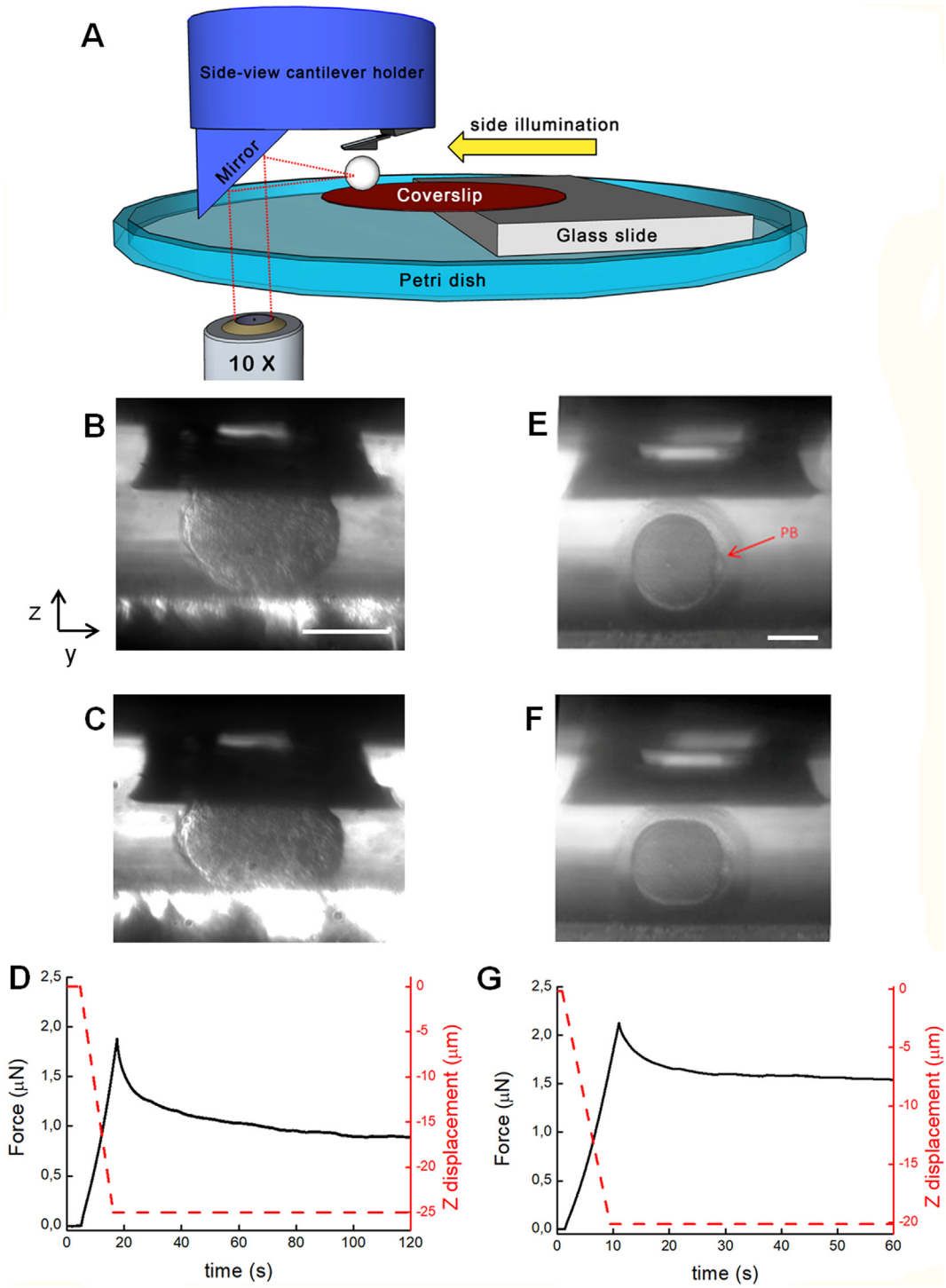

Fig. 3. Scheme illustrating the working principle of side-view cantilever holder (A); side view images of the spheroid confined between the glass cover slip and the AFM macro-probe (B) and the deformed spheroid after the 25 μm downward displacement of the z piezo (C) and the corresponding force relaxation curve (D). Bar 100 μm. Side view images of an healthy MII oocyte, where is clearly visible the first polar body (PB) as indicated by the red arrow, confined between the glass cover slip and the macro-AFM probe (E); deformed oocyte after the 20 μm downward displacement of the z piezo (F) and the corresponding force relaxation curve (G). Bar 50 μm. (For interpretation of the references to colour in this figure legend, the reader is referred to the web version of this article.)

preparation for measurements are reported in Supplemental materials (paragraph 1.1 and 1.2 respectively).

3.2. Analysis of stress-relaxation curves

The behavior of viscoelastic materials under uniaxial loading can be analyzed using a model including both elastic and viscous elements that are combined to describe heterogeneous materials as the case of biological samples. The generalized Maxwell model, consisting of one elastic element and Maxwell elements with parallel arrangement, was observed to be successful in describing force relaxation experiments on a single somatic cell [31] and larger cells such as oocytes [32,33]. In agreement with previous studies, we observed that two Maxwell elements well describe the experimental data both for the oocytes and the 3D spheroids (see Fig. S1). Accordingly we did not increase the number of Maxwell

elements to avoid data overfitting. The model assumes that the cell is subjected to a constant deformation, the contact area does not change during the measurements and the force decays bi-exponentially. The equation used to fit the data is

$$F(t) = a0 + a1\exp\left(\frac{-(t - t0)}{\tau 1}\right) + a2\exp\left(\frac{-(t - t0)}{\tau 2}\right),$$

where $\tau = \eta/E$ (τ is relaxation time, η viscosity and E Young modulus). In order to evaluate the time relaxation constants, all the curves were then fitted by using a Matlab routine. Examples of the data fitting are reported in the Supplementary data (see Fig.S2).

3.3. Analysis of the cell deformation

To have an estimation of the oocyte and the tumor spheroid deformation during stress-relaxation measurements, the percentage of vertical deformation under vertical compression was evaluated. The vertical deformation ($\Delta L/L$) was quantified as the height variation of the object (oocyte/spheroid) during compression (ΔL), divided by the height of the object at the initial stage (L). The height of the oocytes and spheroids was estimated by analyzing the optical side-view images (see Fig. S3).

3.4. Statistical analysis

The statistical difference among the groups of data both for oocytes and tumor spheroids was evaluated by non-parametric ANOVA test, Kruskal-Wallis test with Dunn's multiple comparison test. In all cases, the statistical analysis was performed by GraphPad Prism 5.0. A p value <0.05 was considered to be statistically significant.

4. Mechanical characteristics of 3D cell spheroids and oocytes

The aim of this work is to demonstrate that the AFM macro-probes we fabricated can be easily used to measure the mechanical characteristics of large biological systems by the AFM technique. The AFM macro-probes are tested with 3D multicellular tumor spheroids at different growing stage, with a diameter between 130 and 325 μm, and human oocytes. Multicellular aggregates, as 3D tumor spheroids are very interesting since, better than 2D cultures, reproduce the early tumor environment, and include the cell–cell and the cell-extracellular matrix interactions that affect the mechanical response of the spheroid [34]. Mammalian oocytes are spherical cells having a diameter of about 100 μm with a complex ultra-structure: the ZP, an extracellular glycoprotein layer (thickness 15 μm) that surrounds a perivitelline space, a polar body (at the MII maturation stage), and the ooplasm, where mitotic spindle can have different orientations depending on the maturation stage [35]. All of them can contribute, together with the other cell components, to the mechanical response of this macrocell. A sketch illustrating the set-up of the measurements is shown in Fig. 3A. Representative images of the 3D cell spheroid and the oocyte confined between the probe and the glass support, with the probe at the contact position, are shown in Fig. 3B and 3E. The same samples under maximum compression are shown in Fig. 3C and 3F, together with the corresponding force-relaxation curves (Fig. 3D and 3G). During measurements the status of oocytes or tumor spheroids is monitored in the side-view images. Once the AFM macro-probe is moved back to its initial position, the oocyte/spheroid fully recovers its original shape, and no permanent deformation is observed in both biological systems (see Movies S2, S3).

4.1. Viscoelastic features and structural deformation of 3D cell spheroids

The relaxation time constants ($\tau 1$ and $\tau 2$) of tumor spheroids as a function of their diameter are shown in Fig. 4A: for diameter of 130 μm $\tau 1 = (4 \pm 2)$s and $\tau 2 = (44 \pm 24)$s; for 200 μm $\tau 1 = (4 \pm 1)$s and $\tau 2 = (20 \pm 15)$s; for 300 μm and $\tau 1 = (4.0 \pm 0.9)$s and $\tau 2 = (46 \pm 12)$s; for 325 μm $\tau 1 = (3 \pm 1)$s and $\tau 2 = (30 \pm 19)$s are obtained. No remarkable variations of the relaxation times are observed among spheroids having different diameters.

The presence of a fast and then slow relaxation time has been observed in compression and decompression measurements of various 3D cell spheroids [25,36]. The $\tau 1$ and $\tau 2$ relaxation time values appear to be consistent with those observed for some cell aggregates derived from living embryonic tissues as measured by parallel plate compression apparatus [36]. In this case, the authors have proposed an interpretation of this bimodal relaxation: $\tau 1$ is in the time scale characterizing the relaxation of elastic deformation of individual cell in the aggregate, together with extracellular matrix molecules. The elastic stress is quickly dissipated and is followed by a slow viscous response characterized by the larger relaxation time $\tau 2$ due to movement of individual cells, which break and reform their adhesive contacts with the neighbors and the interior of the aggregate is reorganized [36]. It is known that the cellular organization varies inside the spheroid and depends on the growing stage, as reported in the analysis of structure and physiology of the spheroids [37]. The most proliferating cells are located on the

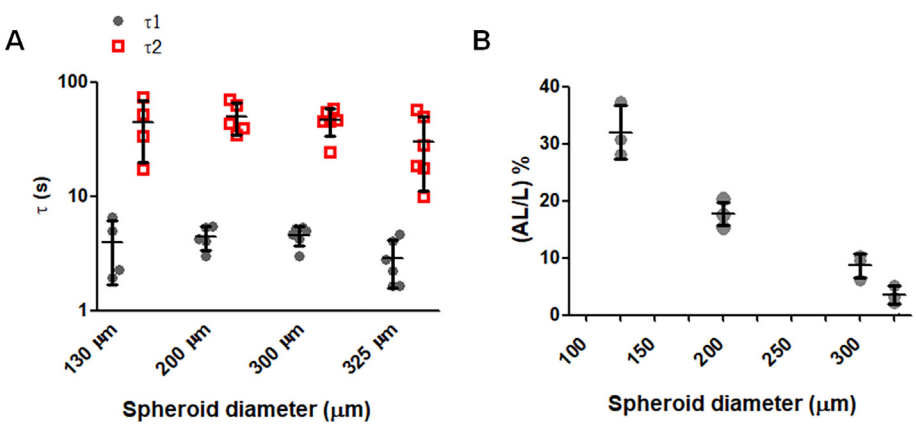

Fig. 4. Values of the constant relaxation time of tumor cell spheroids with different diameter as obtained by fitting the data with the generalized Maxwell model (A). Each dot represents a single curve analyzed; mean (horizontal bar) and SD are superimposed. The values of $\tau 1$ and $\tau 2$ are non significantly different among the spheroids with different size. The corresponding deformation values as function of spheroid diameters, each dot is related to a single image (B).

tumor spheroid surface, where they have an arrangement looser than the inner compact regions, which are demonstrated to be in hypoxic and anoxic state for spheroids having diameter of 250–300 μm [38], or in necrosis for cell spheroid having diameter above 550 μm [37]. In order to characterize the ultrastructure of the measured 3D tumor spheroids, we carry out a TEM analysis (all the details of sample preparation and TEM images are reported in the Supplementary Materials). TEM images at different magnification are acquired on small and large spheroids, obtained by the same culture of those used for mechanical measurements. In agreement to what reported in literature [38] the TEM images show that the small spheroids (below 200 μm) appear as a uniform loose pack of cells aggregate, in which cells do not uniformly adhere to each other. The larger spheroids (above 200 μm) show an external layer, where cells do not closely adhere to each other, and the inner nucleus which consists of closely packed adherent cells (Fig. S4). In these spheroids the presence of a necrotic core was never observed. The TEM images demonstrate that the small spheroids and the external layer of the larger ones exhibit a similar cellular arrangement.

From the analysis of the spheroid deformation, the small spheroids (diameter below 200 μm) appear to deform much more than the larger ones (above 200 μm), as expected for the same vertical compression (Fig. 4B). Since the small 3D tumor spheroids and the external layer of the larger ones share a similar cellular organization (see Fig. S4) this might result in comparable viscoelastic properties. This would suggest that for small deformation of large spheroid (above 200 μm), the viscoelastic response is mainly dominated by the external cellular layer. This layer is generally characterized by highly proliferating cells and this means that two relaxation times obtained can be correlated to the status and rearrangement of the different components of this layer: cell status, cell-cell adhesion and space among them, as also proposed by other authors [36].

The perturbation of these components could be useful to definitively support that the external layer is the portion of the spheroid dominating the mechanical response for small deformations of large tumor spheroids. For instance the culturing at low level of O_2 might interfere with the external layer physiology and proliferation. In alternative one might also alter the cell dynamics and the cell-cell interactions that are related to the external highly proliferating cell region. For instance filamentous actin is an important component of the cytoskeleton that is reported to be more abundant and organized at the periphery of the tumor spheroid than in the intermediate or core region [39].

Multicellular spheroids formed by other tumor cell lines or by non tumor cell lines may show a different behavior, as well different environmental conditions, such as dosing anticancer drugs, may result in a change of the viscoelastic properties. From this point of view, the independence of the relaxation from the spheroid size, when measured with our approach, should be seen as an advantage, since it would allow to discard this effect from future studies.

4.2. Viscoelastic features and structural deformation of human oocytes

By optical microscope inspection the oocytes are identified and classified according to maturation phase as immature (MI), mature (MII) for the presence of polar body, and dysmorphic MII when anomalous morphological characteristics are observed (Fig. 5A). The corresponding relaxation time constants are displayed in Fig. 5B, with a mean value of $\tau1 = (1.3 \pm 0.5)$ s and $\tau2 = (13 \pm 6)$s for MI; $\tau1 = (1.7 \pm 0.7)$s and $\tau2 = (14 \pm 6)$s for MII; $\tau1 = (2.2 \pm 0.6)$s and $\tau2 = (21 \pm 9)$s for dysmorphic MII. The relaxation times values are comparable for the three groups.

In all investigated oocytes we observe two distinct relaxation processes: a fast relaxation (1–2 s) and a second slower relaxation (13–20 s). The presence of two relaxation times suggests that the mechanical response of the oocyte is dominated by different components, as it has been proposed also for somatic cells [31]. The side-view images, acquired during relaxation measurements, show that the compression of the oocyte involves all its main structures: ZP, the perivitelline space and the ooplasm. From the analysis of the images of the oocyte at MII stage, we observe that a vertical displacement of 20 μm, determines a deformation of 11 ± 4% for the whole oocyte (ooplasm + ZP) and 13 ± 3% for the ooplasm. These data further indicate that the main components of the oocyte deform differently under the same compression.

The values of relaxation constant τ1 appear in the same range of those obtained for other mammalian oocytes measured by micropipette aspiration: $\tau = 1.5 \pm 0.5$ s for bovine oocytes [32] and $\tau = 2–4$ s for oocytes retrieved from young and aged mice [40]. However, on fresh mouse oocytes, when mechanical measurements are performed by magnetic tweezers, faster relaxation are observed (0.15 s) [41]. Such variations in the values of cell mechanical features are not unusual. A recent study, performed

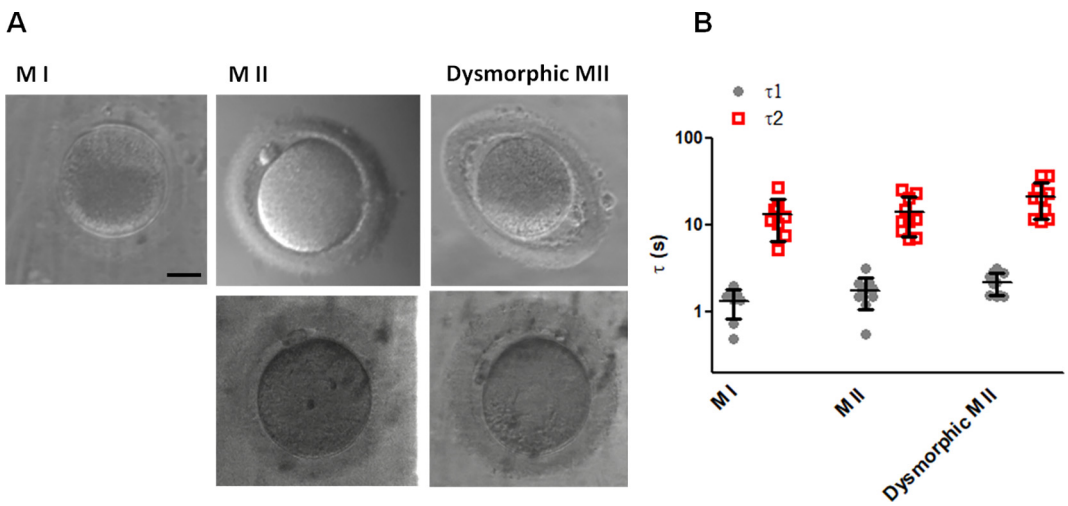

Fig. 5. Bright field images of the oocytes identified and divided according to the maturation stage (M I) (n = 1) and M II (n = 2) and dysmorphic features dysmorphic M II (n = 2) (A); bar 25 μm. The relaxation times of these oocytes as obtained by fitting the curves with the generalized Maxwell model (B). Each dot represents a single curve analyzed; mean (horizontal bar) and SD are superimposed. Among the oocytes the values of τ1 and τ2 are not significantly different.

on a somatic cell, highlights that the mechanical properties of a specific cell line can vary several orders of magnitude depending on time-scale of the measurements, applied stress and deformation rate [42]. In a more recent work, where the whole human oocyte is compressed, the mechanical characterization demonstrates that two relaxation constants can be observed, with τ values comparable with those we have obtained [33]. In this work Shen et al. proposed a reduced model that allows separating the mechanical contribution of ZP from that of the ooplasm. To fully determine the properties of the oocyte, two consecutive measurements by varying the indenter's size are needed. A small indenter can be used to determine the ZP mechanical parameters while a large indenter can provide ooplasm mechanical contribution [33]. In a previous work, to separate the contribution of ZP from the rest of oocyte, AFM indentation measurements are performed on the ZP physically removed from the oocyte. In this case, for 2 μm/s loading rate, a very fast relaxation (0,00134 s) is obtained [43]. Such lower value could be possibly due to structural changes caused by the ZP removal from the oocyte.

According to the model proposed by Shen et al., the AFM macro-probes can provide a characterization of the mechanical behavior of ooplasm without requiring physical removal of ZP. Hence by combining our data with the reduced model we quantify all the elastic modulus (Ec) and the viscosity (ηc) of the ooplasm (all the details about the analysis and results are reported in supplementary materials paragraph 5 and Fig. 5S). Based on this analysis the Ec value is found in agreement with that obtained by Shen et al. Moreover, we observe that the MII ooplasm is softer than the MI, while for the dysmorphic MII the Ec values appear to be widely distributed. By using the fast relaxation time constant, which represents the ooplasm relaxation time according to the reduced model, we evaluate the ηc values, which are observed to be compatible with those found by Shen et al. Interestingly, we also observed that, while MI and MII display a similar ooplasm viscosity values, the dysmorphic oocytes present a higher viscosity than that of MI and MII. These results strongly indicate that the mechanical response is a promising parameter to distinguish competent MII form dysmorphic MII oocyte. In this sense the AFM macro-probes can be very useful to perform more controlled measurements by AFM and to achieve a description of the mechanical response of all components of the oocyte at the different maturation stages and cell status.

In a precedent work we have observed a similar heterogeneous mechanical response of ZP in AFM indentation measurements performed on the whole oocyte, that have provided two distinct elastic modulus values, which have been ascribed to the external superficial layer of ZP and to the inner ZP region and contribution from the rest of the oocyte [12].

The stiffness of human oocytes has been probed in several studies [11,12,23,44], while their viscoelastic features have been quantified in a lower number of studies [11,33]. However, qualitative observations of ooplasm viscosity have demonstrated that it can be used to predict the fate of oocytes after ICSI procedure [45]. Moreover the ooplasm fluidity, correlated with oocyte aging, has been observed to inhibit sperm fusion and likelihood of a successful fertilization [46].

The possibility to obtain a set of measurable mechanical parameters (i.e. stiffness, viscosity and viscoelasticity), which can be correlated with a high chance of oocyte to be fertilized, could represent a very useful indicator to exploit for a non-invasive oocyte selection during in vitro fertilization procedures (IVF) procedures. The positive outcome of IVF strictly depends on the oocyte quality. To date, in clinical practice, the evaluation of oocyte quality still relies on the observation of morphological features, and the result is based on the competence of the embryologist. As demonstrated by us and other authors, the elasticity of the oocyte and ZP can vary according to maturation stage and cell quality [12,23,45]. Nowadays several studies strongly support the idea that the biomechanical properties can represent a non-invasive objective biomarker that could improve the selection of oocytes with high developmental potential [11,12,24,33].

In addition the use of AFM macro-probes, combined with the side-view imaging, could be very useful to study the forces involved in the maturation stages of the oocyte, or in other words in the different phases of the meiosis. In presence of fluorescent dye labeling to detect actin distribution and the actomyosin ring positioning, this approach would allow to identify the role of actin distribution in the mechanical properties of the oocyte.

5. Conclusions

In summary, we designed and fabricated AFM macro-probes compatible with commercial AFM apparatus and with optical side-view visualization set-up. We demonstrated that they are a valuable tool to investigate the mechanical characteristics of large and complex biological systems as mammalian oocytes and 3D cell spheroids. The application of these innovative AFM probes can improve the understanding of the mechanical properties associated with tissue mechanics in the diverse fields as embryology, tissue morphogenesis and oncology.

Acknowledgements

Financial support by Health Ministry (RF-2011-02351812) Ricerca Finalizzata "Applications of Ultrastructural Cell Analysis in the Field of Reproductive Technologies" and by Regione Friuli Venezia Giulia, within the framework of "legge regionale 17/2004: Contributi per la ricerca clinica, traslazionale, di base, epidemiologica e organizzativa", with the project "BioMec – Applicazione delle tecnologie biomeccaniche a integrazione delle metodiche tradizionali nel contesto ospedaliero" are gratefully acknowledged. L.A. and M.L. acknowledge CBM-Consorzio per il Centro di Biomedicina Molecolare S.c.a.r.l. for providing access to the BioNanoAnalysis core facility. M.S.L.G. acknowledges financial support from Area Science Park through the Made in Trieste project. R.C. acknowledges financial support from Basic Research Program 2015, University of Verona (RATs 2015).

We thank Marina Zweyer for useful discussion about TEM images analysis and Roberta Bortul for TEM samples preparation. We are grateful to Edoardo Milotti who, with several discussions on the importance of mechanical properties in biology and on their interpretation, inspired and triggered this work.

Declaration of Competing Interest

The authors declare that they have no conflict of interest.

References

[1] D. Wirtz, K. Konstantopoulos, P.C. Searson, The physics of cancer: the role of physical interactions and mechanical forces in metastasis, Nat. Rev. 11 (2011) 512–522.

[2] N. Bufi, M. Saitakis, S. Dogniaux, O. Buschinger, A. Bohineust, A. Richert, M. Maurin, C. Hivroz, A. Asnacios, Human primary immune cells exhibit distinct mechanical properties that are modified by inflammation, Biophys. J. 108 (2015) 2181–2190.

[3] Y. Qi, L. Andolfi, F. Frattini, F. Mayer, M. Lazzarino, J. Hu, Membrane stiffening by STOML3 facilitates mechanosensation in sensory neurons, Nat. Commun. 6 (2015) 8512.
[4] S.J. Morley, Y. Qi, L. Iovino, L. Andolfi, D. Guo, N. Kalebic, L. Castaldi, C. Tischer, C. Portulano, G. Bolasco, K. Shirlekar, C.M. Fusco, A. Asaro, F. Fermani, M. Sundukova, U. Matti, L. Reymond, A. De Ninno, L. Businaro, K. Johnsson, M. Lazzarino, J. Ries, Y. Schwab, J. Hu, P.A. Heppenstall, Acetylated tubulin is essential for touch sensation in mice, eLife 5 (2016) e20813.
[5] M. Krieg, A.R. Dunn, M.B. Goodman, Mechanical control of the sense of touch by β-spectrin, Nat. Cell Biol. 16 (2014) 224–237.
[6] E.D. Schmell, B.J. Gulyas, J.L. Hedrick, Egg Surface Changes During Fertilization and the Molecular Mechanism of the Block to Polyspermy, New York Academic Press, 1983, p. 365.
[7] O. Otto, P. Rosendahl, A. Mietke, S. Golfier, C. Herold, D. Klaue, S. Girardo, S. Pagliara, A. Ekpenyong, A. Jacobi, M. Wobus, N. Töpfner, U.F. Keyser, J. Mansfeld, E. Fischer-Friedrich, J. Guck, Real-time deformability cytometry: on-the-fly cell mechanical phenotyping, Nat. Methods 12 (2015) 199–202.
[8] M. Islam, H. Brink, S. Blanche, C. Di Prete, T. Bongiorno, N. Stone, A. Liu, A. Philip, G. Wang, W. Lam, A. Alexeev, E.K. Waller, T. Sulchek, Microfluidic sorting of cells by viability based on differences in cell stiffness, Sci. Rep. 7 (2017) 1997.
[9] L. Andolfi, E. Bourkoula, E. Migliorini, A. Palma, A. Pucer, M. Skrap, G. Scoles, A. P. Beltrami, D. Cesselli, M. Lazzarino, Investigation of adhesion and mechanical properties of human glioma cells by single cell force spectroscopy and atomic force microscopy, PloS One 9 (2014) e112582.
[10] A.V. Nguyen, K.D. Nyberg, M.B. Scott, A.M. Welsh, A.H. Nguyen, N. Wu, S.V. Hohlbauch, N.A. Geisse, E.A. Gibb, A.G. Robertson, T.R. Donahue, A.C. Rowat, Stiffness of pancreatic cancer cells is associated with increased invasive potential, Integr. Biol. 8 (2016) 1232–1245.
[11] L.Z. Yanez, D.B. Camarillo, Microfluidic analysis of oocyte and embryo biomechanical properties to improve outcomes in assisted reproductive technologies, Mol. Hum. Reprod. 23 (2017) 235–247.
[12] L. Andolfi, E. Masiero, E. Giolo, M. Martinelli, S. Luppi, S. dal Zilio, I. Delfino, R. Bortul, M. Zweyer, G. Ricci, M. Lazzarino, Investigating the mechanical properties of zona pellucida of whole human oocytes by atomic force spectroscopy, Integr. Biol. 8 (2016) 886–893.
[13] R.M. Hochmuth, Micropipette aspiration of living cells, J. Biomech. 33 (2000) 15.
[14] S. Nawaz, P. Sánche, K. Bodensiek, S. Li, M. Simons, I.A.T. Schaap, Cell visco-elasticity measured with AFM and optical trapping at sub-micrometer deformations, PLoS One 7 (2012) e45297.
[15] G. Coceano, M.S. Yousafzai, W. Ma, F. Ndoye, L. Venturelli, I. Hussain, S. Bonin, J. Niemela, G. Scoles, D. Cojoc, E. Ferrari, Investigation into local cell mechanics by atomic force microscopy mapping and optical tweezer vertical indentation, Nanotechnology 27 (2016) 065102.
[16] M. Krieg, G. Fläschner, D. Alsteens, B.M. Gaub, W.H. Roos, G.J.L. Wuite, H.E. Gaub, C. Gerber, Y.F. Dufrêne, D.J. Müller, Atomic force microscopy-based mechanobiology, Nat. Rev. Phys. 1 (2019) 41–57.
[17] O. Thoumine, A. Ott, Time scale dependent viscoelastic and contractile regimes in fibroblasts probed by microplate manipulation, J. Cell Sci. 110 (1997) 2109–2126.
[18] D.R. Gossetta, H.T.K. Tsea, S.A. Leec, Y. Ying, A.G. Lindgren, Otto O. Yang, J. Raob, A.T. Clark, D. Di Carlo, Hydrodynamic stretching of single cells for large population mechanical phenotyping, PNAS 15 (109) (2012) 7630–7635.
[19] A. Yeung, E. Evans, Cortical shell-liquid core model for passive flow of liquid-like spherical cells into micropipets, Biophys. J. 56 (1989) 139–149.
[20] K. Haase, A.E. Pelling, Investigating cell mechanics with atomic force microscopy, J. R. Soc. Interface 12 (2015) 20140970.
[21] E. Fischer-Friedrich, A.A. Hyman, F. Jülicher, D.J. Müller, J. Helenius, Quantification of surface tension and internal pressure generated by single mitotic cells, Sci. Rep. 4 (2014) 6213.
[22] M. Krause, J. te Riet, K. Wolf, Probing the compressibility of the tumor cell nuclei by combined atomic force-confocal microscopy, Phys. Biol. 10 (2013) 065002.
[23] M. Khalilian, M.R. Valojerdi, M. Navidbakhsh, M. Chizari, P. Eftekhari-Yazdi, Estimating zona pellucida hardness under microinjection to assess oocyte/embryo quality: analytical and experimental studies, Adv. Biosci. Biotechnol. 4 (2013) 679–688.
[24] L.Z. Yanez, J. Han, B.B. Behr, R.A. Reijo Pera, D.B. Camarillo, Human oocyte developmental potential is predicted by mechanical properties within hours after fertilization, Nat. Commun. 7 (2016) 10809.
[25] P. Marmottant, A. Mgharbel, J. Käfer, B. Audren, J.P. Rieu, J.C. Vial, B. van der Sanden, A.F. Marée, F. Graner, H. Delanoë-Ayari, The role of fluctuations and stress on the effective viscosity of cell aggregates, Proc. Natl. Acad. Sci. U.S.A. 106 (41) (2009) 17271–17275.
[26] E.-M. Schötz, M. Lanio, J.A. Talbot, M.L. Manning, Glassy dynamics in three-dimensional embryonic tissues, J. R. Soc. Interface 10 (2013) 20130726.
[27] W.S. Wang, M. Lin, Y. Han, G. Zhao, T.J. Lu, F. Xu, Advances in Experimental approaches for investigating cell aggregate mechanics, Acta Mech. Solida Sin. 25 (2012) 473–482.
[28] S. Bhat, D. Jun, B.C. Paul, T.E.S. Dahms, Viscoelasticity – From Theory to Biological Applications Edition Chapter 6, InTech Editors, 2012, pp. 123–156.
[29] M.P. Stewart, A.W. Hodel, A. Spielhofer, C.J. Cattin, D.J. Müller, J. Helenius, Wedged AFM-cantilevers for parallel plate cell mechanics, Methods 60 (2013) 186–194.
[30] R.S. Gates, M.G. Reitsma, Precise atomic force microscope cantilever spring constant calibration using a reference cantilever array, Rev. Sci. Instrum. 78 (2007) 086101.
[31] S. Moreno-Flores, R. Benitez, M.M. Vivanco, J.L. Toca-Herrera, Stress relaxation and creep on living cells with the atomic force microscope: a means to calculate elastic moduli and viscosities of cell components, Nanotechnology 21 (2010) 445101.
[32] S. Sakuma, B. Turan, F. Arai, High throughput mechanical characterization of oocyte using robot integrated microfluidic, in: IEEE/RSJ International Conference on Intelligent Robots and Systems, 2013, p. 2047.
[33] T. Shen, E. Benet, S.L. Sridhar, J. Abadie, E. Piat, F.J. Vernerey, Separating the contributions of zona pellucida and cytoplasm in the viscoelastic response of human oocytes, Acta Biomater. 85 (2019) 253–262.
[34] G. Lazzari, V. Nicolas, M. Matsusaki, M. Akashi, P. Couvreur, Simona Mura, Multicellular spheroid based on a triple co-culture: a novel 3D model to mimic pancreatic tumor complexity, Acta Biomater. 78 (2018) 296–307.
[35] R. Li, D.F. Albertini, The road to maturation: somatic cell interaction and self-organization of the mammalian oocyte, Nat. Rev. 14 (2013) 141–152.
[36] G. Forgacs, R.A. Foty, Y. Shafrir, M.S. Steinberg, Viscoelastic properties of living embryonic tissues: a quantitative study, Biophys. J. 74 (1998) 2227–2234.
[37] S. Riffle, R.N. Pandey, M. Albert, R.S. Hegde, Linking hypoxia, DNA damage and proliferation in multicellular tumor spheroids, BMC Cancer 17 (2017) 338.
[38] S.-M. Ong, Z. Zhao, T. Arooz, D. Zhao, S. Zhang, T. Du, M. Wasser, D. Van Noort, H. Yu, Engineering a scaffold-free 3D tumor model for in vitro drug penetration studies, Biomaterials 31 (2010) 1180–1190.
[39] W. Lee, Ni. Kalashnikov, S. Mok, R. Halaoui, E. Kuzmin, A.J. Putnam, S. Takayama, M. Park, L. McCaffrey, Ru. Zhao, R.L. Leask, C. Moraes, Dispersible hydrogel force sensors reveal patterns of solid mechanical stress in multicellular spheroid cultures, Nat Commun. 10 (2019) 144.
[40] X. Liu, J. Shi, Z. Zong, K.-T. Wan, Y. Sun, Elastic and viscoelastic characterization of mouse oocytes using micropipette indentation, Ann. Biomed. Eng. 40 (2012) 2122–2130.
[41] B.G. Hosu, S.F. Mullen, J.K. Critser, G. Forgacs, Reversible disassembly of the actin cytoskeleton improves the survival rate and developmental competence of cryopreserved mouse oocytes, PloS One 3 (2008) e2787.
[42] P. Wu, D. Raz-Ben Aroush, A. Asnacios, W.-C. Chen, M.-E. Dokukin, B.L. Doss, P. Durand-Smet, A. Ekpenyong, J. Guck, N.V. Guz, P.A. Janmey, J.S.H. Lee, N.M. Moore, A. Ott, Y.-C. Poh, R. Ros, M. Sander, I. Sokolov, J.R. Staunton, N. Wang, G. Whyte, D. Wirtz, A comparison of methods to assess cell mechanical properties, Nat. Methods 15 (2018) 491–498.
[43] A. Boccaccio, L. Lamberti, M. Papi, M. De Spirito, C. Douet, G. Goudet, C. Pappalettere, A hybrid characterization framework to determine the visco-hyperelastic properties of a porcine zona pellucid, Interface Focus 4 (2014) 20130066.
[44] Y. Murayama, J. Mizuno, H. Kamakura, Y. Fueta, H. Nakamura, K. Akaishi, K. Anzai, A. Watanabe, H. Inui, S. Omata, Mouse zona pellucida dynamically changes its elasticity during oocyte maturation, fertilization and early embryo development, Hum. Cell. 19 (2006) 119–125.
[45] T. Ebner, M. Moser, M. Sommergruber, M. Puchner, R. Wiesinger, G. Tews, Developmental competence of oocytes showing increased cytoplasmic viscosity, Human Reprod. 18 (2003) 1294–1298.
[46] T. Takahashi, E. Takahashi, H. Igarashi, N. Tezuka, H. Kurachi, Impact of oxidative stress in aged mouse oocytes on calcium oscillations at fertilization, Mol. Reprod. Dev. 66 (2003) 143–152.